

Structure of the Yeast Cytochrome bc_1 Complex with a Hydroxyquinone Anion Q_o Site Inhibitor Bound*

Received for publication, March 3, 2003, and in revised form, May 30, 2003
Published, JBC Papers in Press, June 2, 2003, DOI 10.1074/jbc.M302195200

Hildur Palsdottir‡, Carlos G. Lojero§, Bernard L. Trumpower¶, and Carola Hunte‡¶

From the ‡Abt. Molekulare Membranbiologie, Max-Planck-Institut für Biophysik, Marie-Curie-Strasse 15, D-60439 Frankfurt, Germany, §Departamento de Bioquímica, Centro de Investigación y Estudios Avanzados del IPN, Mexico City, c.p. 07360, Mexico and ¶Department of Biochemistry, Dartmouth Medical School, Hanover, New Hampshire 03755

Bifurcated electron transfer during ubiquinol oxidation is the key reaction of cytochrome bc_1 complex catalysis. Binding of the competitive inhibitor 5-*n*-heptyl-6-hydroxy-4,7-dioxobenzothiazole to the Q_o site of the cytochrome bc_1 complex from *Saccharomyces cerevisiae* was analyzed by x-ray crystallography. This alkyl-hydroxydioxobenzothiazole is bound in its ionized form as evident from the crystal structure and confirmed by spectroscopic analysis, consistent with a measured $pK_a = 6.1$ of the hydroxy group in detergent micelles. Stabilizing forces for the hydroxyquinone anion inhibitor include a polarized hydrogen bond to the iron-sulfur cluster ligand His¹⁸¹ and on-edge interactions via weak hydrogen bonds with cytochrome *b* residue Tyr²⁷⁹. The hydroxy group of the latter contributes to stabilization of the Rieske protein in the *b*-position by donating a hydrogen bond. The reported pH dependence of inhibition with lower efficacy at alkaline pH is attributed to the protonation state of His¹⁸¹ with a pK_a of 7.5. Glu²⁷², a proposed primary ligand and proton acceptor of ubiquinol, is not bound to the carbonyl group of the hydroxydioxobenzothiazole ring but is rotated out of the binding pocket toward the heme b_L propionate A, to which it is hydrogen-bonded via a single water molecule. The observed hydrogen bonding pattern provides experimental evidence for the previously proposed proton exit pathway involving the heme propionate and a chain of water molecules. Binding of the alkyl-6-hydroxy-4,7-dioxobenzothiazole is discussed as resembling an intermediate step of ubiquinol oxidation, supporting a single occupancy model at the Q_o site.

Ubiquinol:cytochrome *c* oxidoreductase (cytochrome bc_1 complex, EC 1.10.2.2 (bc_1 complex)) is a multisubunit membrane protein complex, which is one of the fundamental components of respiratory and photosynthetic electron transfer chains. The enzyme catalyzes electron transfer from ubiquinol to cytochrome *c* and couples this process to electrogenic translocation of protons across the membrane (1, 2). Each functional unit of

the homodimeric complex consists of three catalytic subunits: cytochrome *b* with two *b* type hemes, cytochrome c_1 with one *c* type heme, and the Rieske protein containing a [2Fe-2S] cluster. Mitochondrial bc_1 complexes contain up to eight additional subunits. Structures of vertebrate and yeast bc_1 complexes were determined, providing a breakthrough in understanding the enzyme mechanism and structure-function relationships within the enzyme (3–7). The 2.3-Å resolution structure from the yeast *Saccharomyces cerevisiae* has the highest resolution available so far. It allowed a detailed description of substrate and inhibitor binding sites, elucidating parts of the enzyme mechanism and suggesting pathways for proton transfer.

The mechanism of the enzyme known as the protonmotive Q cycle (8) involves separate catalytic sites for ubiquinol oxidation (Q_o site) and ubiquinone reduction (Q_i site). Protons are taken up from the matrix side when ubiquinone is reduced and released to the intermembrane side when ubiquinol is oxidized. The key reaction, ubiquinol oxidation, involves a bifurcated electron transfer. One electron is passed via the [2Fe-2S] cluster to heme c_1 , subsequently reducing the substrate cytochrome *c*. The electron transfer to cytochrome c_1 involves a large scale domain movement of the extrinsic part of the Rieske protein (4). The second electron from ubiquinol is transferred via the low and the high potential *b* type hemes to ubiquinone. The resulting stable semiquinone is fully reduced after a second ubiquinol molecule is oxidized at the Q_o site.

Whereas the main features of catalysis are understood, the molecular mechanism of ubiquinol oxidation is not clear. Also, pathways for proton uptake and release are hypothetical (7, 9, 10). Several hypotheses have been proposed to explain the divergent transfer of electrons into thermodynamically different pathways (see Ref. 2). The double occupancy model suggests synergistic interaction between two quinone molecules that occupy the Q_o site simultaneously (11–13). The proton-gated charge transfer mechanism proposes that the activation barrier is a function of the deprotonation of ubiquinol (14), but this mechanism is not supported by other kinetic studies (15). Single occupancy models include simultaneous as well as sequential electron transfer to the acceptors. For the latter, a proton-gated affinity change mechanism claims the presence of a relatively stable intermediate in the transition state with the rate-limiting step at the second electron transfer (16). Since a semiquinone radical has not been detected at the Q_o site, this has been explained by an EPR silent anti-ferromagnetically coupled semiquinone-[2Fe-2S]^{reduced} pair (16, 17). Another explanation for the undetectable semiquinone is provided by Crofts *et al.* (10, 18), who suggest rapid dissociation of the product after the first electron transfer and movement of the semiquinone within the bilobal Q_o binding pocket to allow rapid reduction of heme b_L . Recent kinetic data show that the midpoint potentials of *b* type hemes control the rate of cyto-

* This work was supported by Deutsche Forschungsgemeinschaft Grant SFB 472, the Max-Planck Gesellschaft, and National Institutes of Health Research Grant GM 20379. The costs of publication of this article were defrayed in part by the payment of page charges. This article must therefore be hereby marked "advertisement" in accordance with 18 U.S.C. Section 1734 solely to indicate this fact.

The atomic coordinates and structure factors (code 1P84) have been deposited in the Protein Data Bank, Research Collaboratory for Structural Bioinformatics, Rutgers University, New Brunswick, NJ (<http://www.rcsb.org/>).

¶ To whom correspondence should be addressed. Tel.: 49-69-6303-1062; Fax: 49-69-6303-1002; E-mail: carola.hunte@mpibp-frankfurt.mpg.de.

chrome c_1 reduction. This is consistent with the view that ubiquinol oxidation is a concerted reaction (19).

Inhibitors are important tools to analyze the molecular mechanism of Q_o site catalysis. Three types of inhibitors can be distinguished: ligands binding at the proximal domain and therefore perturbing the spectroscopic properties of heme b_L (Q_o -I; e.g. myxothiazol and MOA-stilbene), those binding to the distal domain and affecting the Rieske [2Fe-2S] EPR line shape (Q_o -II; e.g. UHDBT),¹ or compounds exhibiting both effects (Q_o -III; e.g. stigmatellin) (20). Kinetic data indicate that occupation of these inhibitors at the Q_o site is mutually exclusive, suggesting overlapping binding sites. This was observed in crystal structures where these inhibitors are found to bind in different but overlapping domains of the bilobal Q_o site, termed distal and proximal to heme b_L (20).

Analysis of anomalous scattering data indicated a high occupancy of the catalytic Rieske domain in the b-position in the presence of inhibitors that bind to the distal domain, such as stigmatellin and UHDBT (20). However, in previous crystallographic studies on UHDBT binding (18, 20), the inhibitor could not be refined, and high resolution structural information about UHDBT binding at the active site has not been available up to now. The substrate ubiquinol has not been detected in the Q_o site by x-ray structural analysis. Therefore, the analysis of structural analogs of the substrate that function as competitive inhibitors is important.

Here, we present the three-dimensional structure of a UHDBT analog, HHDBT-inhibited bc_1 complex from the yeast *S. cerevisiae* at 2.5-Å resolution. This hydroxyquinone binds in its ionized form, and its binding is discussed as resembling an intermediate step of ubiquinol oxidation. Conformational changes at the binding site confirm the previously postulated proton transfer pathway and reveal plasticity at the active site.

EXPERIMENTAL PROCEDURES

Protein Purification and Crystallization—The bc_1 complex from the yeast *S. cerevisiae* was purified, and a co-complex with the antibody fragment Fv_{18E11} was formed and crystallized as previously described with the following minor modifications (6, 21). The buffer volume for detergent exchange in the second DEAE anion exchange chromatographic step was reduced by 5-fold. HHDBT was added at a final concentration of 100 μ M to the purified bc_1 complex-Fv co-complex after size exclusion chromatography (TSK4000; TosoHaas) prior to crystallization. The final purification step was performed at pH 7.5. The crystals were obtained using a microseeding and vapor diffusion technique against polyethylene glycol 4000 at 4 °C. The protein solution (50 mg/ml) was mixed with precipitation agent (5% polyethylene glycol 4000, Tris-HCl pH 7.5 (adjusted at room temperature), 0.05% *n*-undecyl- β -D-maltopyranoside, 10 μ M HHDBT), resulting in a pH of 8.0 at 4 °C; i.e. 0.5 pH unit lower than the structure of the stigmatellin-inhibited enzyme (6). Crystals grew within a few days to a size suitable for x-ray analysis ($\sim 0.5 \times 0.5 \times 1.0$ mm).

Total protein determination was performed with a modified Lowry procedure, using the BC Assay protein quantitation kit (Uptima) (22). The bc_1 complex content was estimated as half the amount from spectroscopic quantification of the two b-type hemes using an extinction coefficient of 28.5 $\text{mM}^{-1} \text{cm}^{-1}$ for the dithionite-reduced minus ferricyanide-oxidized difference spectra (262–275 nm). Enzyme activity was determined by monitoring cytochrome c reduction in a spectrophotometric assay at 550 nm using an extinction coefficient of 18.5 $\text{mM}^{-1} \text{cm}^{-1}$ for cytochrome c . Turnover numbers refer to mol of cytochrome c reduced mol^{-1} of bc_1 complex s^{-1} under conditions of continuous turnover, where the catalytic reaction is zero order with respect to decyl ubiquinol and cytochrome c . A detailed description is reported elsewhere (21).

pK_a Determination of Hydroxydioxobenzothiazoles—For determination of the pK_a in detergent micelles, the longer tridecyl side chain analog was used to retain partitioning of the inhibitor into the micelle. THDBT was dissolved at 5 μ M in a buffered mixture containing 20 mM MES, 20 mM MOPS, 20 mM TAPS, 100 mM NaCl, and 400 μ M *n*-dodecyl- β -D-maltopyranoside, pH 3.5. The pH was adjusted by increments of 0.2–0.5 pH units from pH 3.5 to 8.5 by adding 5 M KOH. Optical spectra were recorded from 250–350 nm with a slit width of 1.5 nm on a computerized DW2a dual wavelength spectrophotometer controlled by OLIS software (On-Line Instruments Systems, Bogart, GA).

Determination of the Apparent K_m of Yeast bc_1 Complex for Ubiquinol in the Absence and Presence of UHDBT—The reaction mixture consisted of 25 μ M cytochrome c in 50 mM potassium phosphate, pH 7, 250 mM sucrose, 1 mM sodium azide, 200 μ M EDTA, and 0.01% Tween 20. Prior to the reaction, the complex was diluted to 15 μ M in the same buffer and incubated for ~ 45 min on ice. The concentration of decyl ubiquinol was varied, and the activity was measured in the absence or presence of UHDBT.

Determination of the Ionization State of Bound THDBT—The bc_1 complex was diluted to a concentration of 2.84 μ M in a buffer at pH 6.0 (50 mM MES, 50 mM MOPS, 50 mM TAPS, 250 mM sucrose, 200 μ M EDTA, 2 mM NaN_3 , 0.1% Tween 20). The complex had an absorbance at 280 nm = 2.7 and a 280:414 absorbance ratio of 3. Spectra were recorded from 250 to 350 nm on the DW2a dual wavelength spectrophotometer. In order to obtain maximum illumination, the slit was set at 6 nm, and the UV filter, quartz diffuser and beam scrambler were removed from the spectrophotometer.

Data Collection and Refinement—X-ray diffraction data were collected at 4 °C at the synchrotron beamline ID14EH3 at the European Synchrotron Radiation Facility (Grenoble, France), using a charge-coupled device detector (marCCD; Mar USA, Evanston, IL). Data were processed with the program DENZO and merged using SCALEPACK from the HKL package (HKL Research, Charlottesville, NC) (23). The crystals belong to the space group C2, with unit cell parameters $a = 215.0$ Å, $b = 165.1$ Å, $c = 147.5$ Å, and $\beta = 117.3^\circ$. The structure was refined using the coordinates of the stigmatellin-inhibited enzyme as a model (Protein Data Bank code 1KB9) after excluding all nonprotein molecules (7). Energy minimization and B-factor refinement were performed using the CNS program package (version 1.0) (24). The maximum likelihood function was used as the target for refinement. The model was improved based on $F_o - F_c$ and $3F_o - 2F_c$ electron density maps, using the program O (version 8.0.4) (25). Amino acid displacements were manually adjusted, followed by stepwise inclusion of the energy-minimized structure of the inhibitor HHDBT, UQ6, phospholipids, and UM and finally manually repositioning a displaced loop. Each step of model building was followed by a refinement cycle. Topology and parameter files were generated using the program Xplo2d and torsion data blocks prepared with the program Moleman2 (X-UTIL package; available on the World Wide Web at x-ray.bmc.uu.se/usf/) (26). The difference electron density map ($F_o - F_c$) indicated the presence of several additional phospholipids, manifested as elongated hairpin-like features. One phospholipid bound close to the Q_o site was identified and refined in addition to the previously assigned phospholipids (7). Finally, water molecules were included according to peaks observed in the $F_o - F_c$ electron density map contoured at 3σ . Their positions were refined yielding 326 molecules of which 203 are the same as in the original model (1KB9), and their numbering was kept. New water molecules were numbered as starting from Wat⁵⁰⁰. Refinement resulted in final R factor and free R factor of 22.8 and 25.2%, respectively (Table I). Coordinates of the HHDBT-inhibited enzyme have been deposited in the Protein Data Bank data base (entry 1P84).

For comparison, stigmatellin-inhibited bc_1 complex was crystallized at the same pH as the HHDBT-containing enzyme. The control data set was collected with 2.8-Å resolution, 93% completeness, and R_{sym} of 5.8%. Refinement resulted in final R factor of 20.8% and R_{free} of 24.5%. Lowering the pH by 0.5 units does not affect the structure of the catalytic subunits of the stigmatellin-inhibited enzyme, as judged by positional root mean square deviation (rmsd; Å) of superimposed atoms with LSQMAN yielding rmsd_{all}/rmsd_{C α} of 0.142/0.098, 0.175/0.118, and 0.204/0.133 for cytochrome b , cytochrome c_1 , and the Rieske protein, respectively (Dejavuu package; available on the World Wide Web at x-ray.bmc.uu.se/usf/). Comparison between the HHDBT- and the stigmatellin-inhibited enzyme was therefore based on the recently published 2.3-Å resolution structure (1KB9) (6). The structures were superimposed using the explicit least squares option in LSQMAN and inspected in the program O. By-residue analysis of root mean square deviation in C α trace position and orientation was performed using the McLachlan algorithm as implemented in the program ProFit version

¹ The abbreviations used are: UHDBT, 5-*n*-undecyl-6-hydroxy-4,7-dioxobenzothiazole; HHDBT, 5-*n*-heptyl-6-hydroxy-4,7-dioxobenzothiazole; THDBT, 5-*n*-tridecyl-6-hydroxy-4,7-dioxobenzothiazole; UM, *n*-undecyl- β -D-maltopyranoside; UQ6, coenzyme Q_6 ; MES, 4-morpholinethanesulfonic acid; MOPS, 4-morpholinepropanesulfonic acid; TAPS, 3-[[2-hydroxy-1,1-bis(hydroxymethyl)ethyl]amino]-1-propanesulfonic acid.

TABLE I
Data collection and refinement statistics

Diffraction data were collected at ESRF, ID14-EH3 at 4 °C, λ 0.9299 Å.

Parameter	Value
Space group	C2
<i>a</i> , <i>b</i> , <i>c</i> [Å]	215.0 165.1 147.5
β (degrees)	117.3
No of nonhydrogen atoms in the model	
Atoms	18,069
Amino acid residues	2169
Nonprotein molecules	13
Solvent molecules	326
Data collection	
Resolution range (outer shell) [Å]	25.0-2.50 (2.56-2.50)
Measured reflections	372,220 (19,194)
Unique reflections	149,103 (9128)
Completeness (%)	92.4 (84.6)
R_{merge} (%) ^a	6.6 (37.3)
$I/\sigma(I) < 1$	13.4 (1.2)
Refinement	
Resolution range (outer shell) (Å)	25.0-2.50 (2.52-2.50)
R factor (%) ^b	22.8 (41.0)
R_{free} (%) ^c	25.2 (41.1)
B_{wilson} [Å ²] ^d	50.3
Average B -factor	72.0
Root mean square deviations from ideal values	
Bond lengths [Å]	0.007
Bond angles (degrees)	1.298
Ramachandran plot (non-Gly, non-Pro)	
Most favored regions (%)	86.8
Additional allowed (%)	12.5
Generously allowed (%)	0.5
Disallowed (%)	0.2

^a $R_{\text{merge}} = \frac{\sum_h \sum_i |I_i(h) - \langle I(h) \rangle|}{\sum_h \sum_i I_i(h)}$, where $I_i(h)$ is intensity of i th measurement, $\langle I(h) \rangle$ is average intensity of a reflection.

^b R factor = $\frac{\sum_h |F(h)_{\text{obs}} - |F(h)_{\text{calc}}||}{\sum_h |F(h)|}$.

^c R_{free} calculated for 2.5% of reflections.

^d B_{wilson} was calculated using TRUNCATE, CCP4 package (53). PDB entry: 1P84.

2.2 (available on the World Wide Web at bioinf.org.uk/software/profit).

Analysis of neighboring atoms and hydrogen bond interactions was performed using the program HBPlus (27) and contact analysis from CNS. Accessibility was estimated, and buried surface calculations were performed using the program NACCESS (28). PROCHECK (version 3.2) analysis verified the stereochemical quality of the coordinates (Table I) (29). Hydrogen bonds were assigned according to appropriate distance and geometry. For analysis of weak hydrogen bonds, an estimation of hydrogen atom position was made by generating a structural model with hydrogens added using CNS (version 1.0). Criteria for identifying weak hydrogen bonds were extracted from Ref. 30. Hydrogen bond angle is denoted as θ (X-H...A), and the bending angle at acceptor atom is shown as ϕ (H...A-C). Figures were prepared using the programs O (25), LIGPLOT version 4.0 (31), MolScript version 1.4 (32), BobScript (33), and Raster3D (34).

RESULTS

Crystallization of HHDBT-inhibited *bc*₁ Complex—The optimized purification of yeast *bc*₁ complex resulted in a pure and more active membrane protein complex with a higher turnover number of 82 s⁻¹ compared with the previously reported activity of 64 s⁻¹ (21). The increase is most likely due to higher phospholipid content of the modified protein preparation (Fig. 1) (35, 36). Effective inhibition of the complex has been shown for 5-*n*-alkyl-6-hydroxy-4,7-dioxobenzothiazoles containing 7–15 carbon alkyl side chains (37). Here, the shorter heptyl side chain analog of UHDBT was used for crystallization in order to avoid nonspecific binding that might occur with the longer alkyl side chains at the high concentrations used.

The inhibitory efficacy of UHDBT was shown to depend on the oxidation-reduction poise of the catalytic subunits, demonstrated by enhanced binding when the Rieske protein is reduced (37). The purified *bc*₁ complex used in this study has a

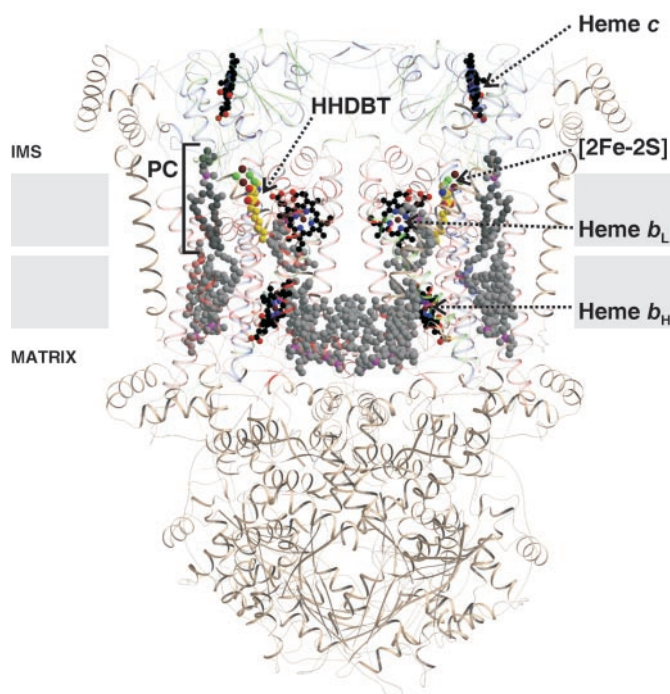


FIG. 1. The structure of the dimeric *bc*₁ complex depicted as a ribbon diagram. Ligands are shown as ball and stick models. HHDBT (yellow) is bound at the Q_o site between the [2Fe-2S] cluster and the heme b_L. Tightly bound phospholipid molecules (gray) are mainly present in the matrix-oriented leaflet of the phospholipid bilayer. The newly identified phosphatidylcholine molecule (PC, dark gray) at the intermembrane side marks the position of the enzyme with respect to the bilayer.

partially reduced Rieske and is fully inhibited by the applied amount of HHDBT (results not shown). A pK_a of 6.5 has been determined for the weakly acidic hydroxy group of UHDBT, which was measured in phosphate buffer containing 1% ethanol, and deprotonation of the hydroxy group is manifested by a color change from yellow to rose-violet (38). Here, the complex was crystallized at pH 8.0 as a protein-detergent complex; therefore, the acidity of the hydroxy group was measured in detergent micelles by monitoring the blue shift in the optical spectrum upon ionization. The pK_a determined by spectrophotometric titration in detergent micelles was 6.1 (results not shown). This suggests that 98% of the inhibitor is ionized in the crystallization mixture, demonstrated by the violet color of the solution and finally a purple tint of the crystals.

A difference spectrum of *bc*₁ complex with bound inhibitor versus the complex alone shows that the inhibitor is ionized when bound to the enzyme, when the pH of the buffer is close to the pK_a of the unbound inhibitor (Fig. 2). The difference spectrum of the complex at pH 6.0 with inhibitor bound at a substoichiometric amount is similar to that of the inhibitor alone at pH 8.7. As inhibitor is added in molar excess, the mixture consists of bound and unbound inhibitor, and the absorbance maximum shifts to longer wavelengths.

Analysis of HHDBT Binding at the Q_o Site—The difference electron density map ($F_o - F_c$) calculated prior to inclusion of HHDBT clearly showed the localization of the bound inhibitor at the Q_o site (Figs. 1 and 3). The clear cut and asymmetric form of the difference density for the head moiety allowed unambiguous orientation of the hydroxydioxobenzothiazole ring. Furthermore, the position of the alkyl side chain was defined in the full length.

The inhibitor binds in the distal domain of the Q_o site, located between the two electron acceptors of ubiquinol oxidation, namely heme b_L and the [2Fe-2S] cluster of the Rieske

FIG. 2. **Ionization of hydroxydioxobenzothiazole bound to yeast *bc*₁ complex.** Left panel, spectra of 5 μ M THDBT at pH 6.0 and 8.7. Ionization of the 6-hydroxy group shifts the absorbance maximum from 284 to 272 nm. Right panel, difference spectra recorded after adding 1.6, 2.3, and 3.6 μ M THDBT to yeast *bc*₁ complex. The enzyme was diluted to a concentration of 2.84 μ M in a buffer at pH 6.0 and divided between two cuvettes. Difference spectra were recorded as the inhibitor was added to one cuvette. Lowering THDBT concentration to substoichiometric amounts shifts the absorbance maximum to 272 nm, indicating ionization of the bound inhibitor.

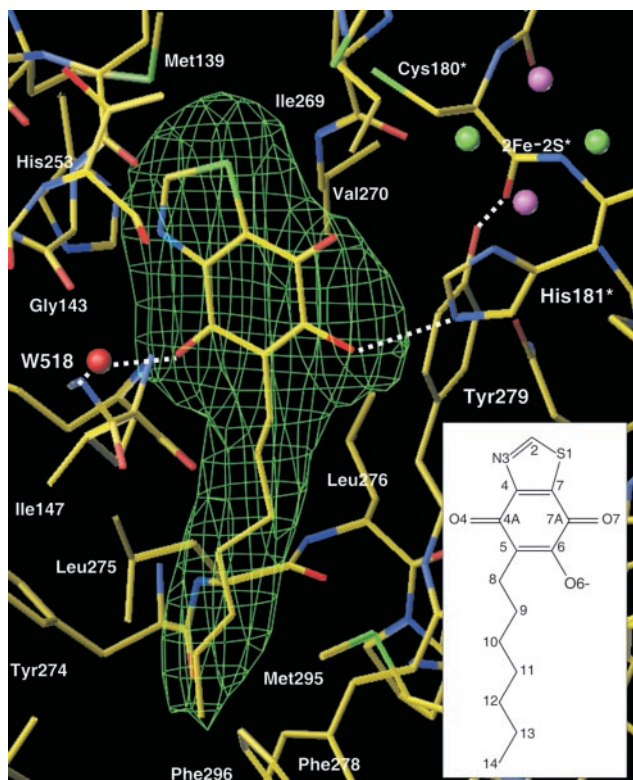
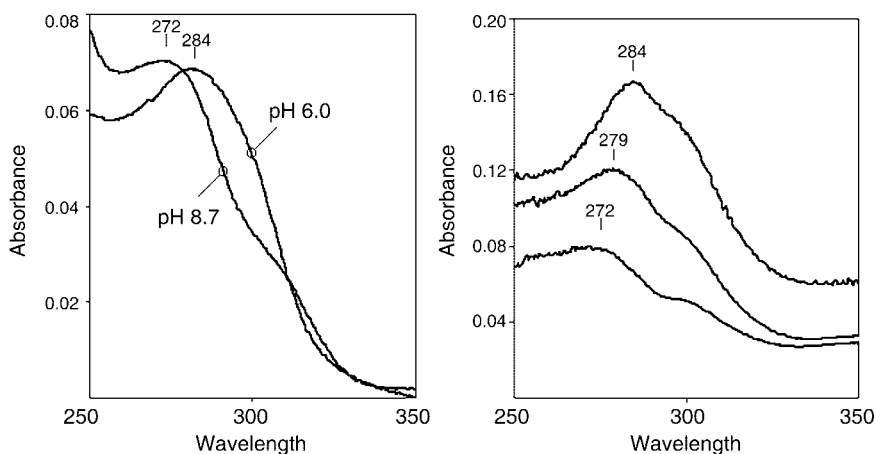


FIG. 3. **HHDBT binding at the *Q*_o site of yeast *bc*₁ complex.** The difference density map was calculated ($F_o - F_c$) before inclusion of the ligand and is contoured at 3σ . It allows unambiguous orientation of HHDBT, which is shown in the final refined model. Residues that stabilize ligand binding and are visible in this orientation are labeled. His^{181*}, a coordinating ligand of the [2Fe-2S] cluster, is within hydrogen bond distance to the hydroxyl oxygen. The carbonyl oxygen atom forms a hydrogen bond to a water molecule Wat⁵¹⁸. Atoms are shown in standard colors. Atom numbering of the hydroxyquinone anion is depicted in the inset.

protein. The catalytic domain of the latter is docked onto cytochrome *b* (*i.e.* in the *b*-position). The hydroxydioxobenzothiazole head group is stabilized by a network of weak and strong hydrogen bonds and numerous van der Waals interactions with neighboring residues (Table II). Importantly, the oxygen atom of the ionized 6-hydroxy group (O6) is in close contact with the nitrogen atom Ne2 of His¹⁸¹, of which the second imidazole nitrogen coordinates the [2Fe-2S] cluster of the Rieske protein. The distance and geometry of the interaction ($d_{N\epsilon 2-O6} = 2.8$ Å; $\theta = 148^\circ$) are in good agreement with a conventional hydrogen bond.

Crystallographic analysis of stigmatellin binding clearly

TABLE II
Contacts between cytochrome *bc*₁ complex residues and inhibitor (*inh*) atoms

Distances less than 3.9 Å are shown.

Cobp	Å	inh.
Met ¹³⁹ (O)	3.6	C2
Trp ¹⁴² (C)	3.9	C2
	3.9	S1
Trp ¹⁴² (C β)	3.8	S1
Trp ¹⁴² (O)	3.9	S1
Gly ¹⁴³ (N)	3.4	C2
	3.8	N3
Gly ¹⁴³ (C α)	3.5	N3
	3.6	C2
Val ¹⁴⁶ (C β)	3.8	O7
	3.9	C7
Val ¹⁴⁶ (C γ 1)	3.6	O7
	3.7	C7
	3.6	O6
	3.7	C6
Val ¹⁴⁶ (C γ 2)	3.2	O7
	3.7	C7
Ile ¹⁴⁷ (C δ 1)	3.4	C9
Ile ²⁶⁹ (C δ 1)	3.7	S1
	3.6	C7A
	3.8	C7
	3.9	O7
Pro ²⁷¹ (C β)	3.4	O4
	3.7	C4
Pro ²⁷¹ (C γ)	3.6	C4
	3.7	O4
	3.8	C5
Phe ²⁷⁸ (C β)	3.9	C12
Tyr ²⁷⁹ (C δ 1)	3.2	O6
	3.7	C6
Tyr ²⁷⁹ (C ϵ 1)	3.3	O6
	3.7	C6
Ile ²⁹⁹ (C δ 1)	3.9	C14
Rip1p	Å	inh.
Cys ¹⁸⁰ (C β)	3.8	O7
His ¹⁸¹ (C ϵ 1)	3.4	O7
	3.6	O6
His ¹⁸¹ (C δ 2)	3.9	O6
His ¹⁸¹ (N ϵ 2)	2.8	O6
	3.5	O7
Water	Å	inh.
Wat ⁵¹⁸	2.9	O4

showed that Ne2 is protonated at pH 8.5, since the fixation of the Rieske protein in the *b*-position is stabilized by a hydrogen bond between this atom and the carbonyl group of stigmatellin (6). For crystallization of the *bc*₁ complex in the presence of HHDBT, the pH was lowered by half a unit; therefore, Ne2 is expected to be protonated under these conditions (see "Discus-

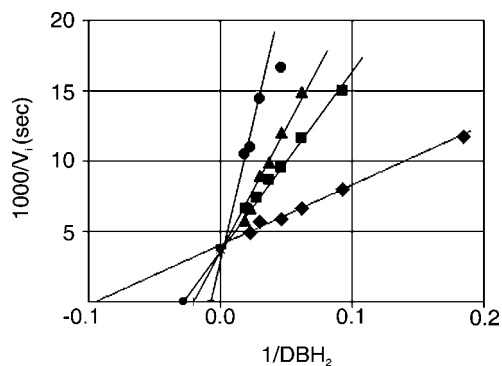


FIG. 4. Lineweaver-Burk plot for determination of the apparent K_m of yeast bc_1 complex for ubiquinol in the absence and presence of UHDBT. The concentration of decyl ubiquinol was varied from 5 to 54 μM , and the activity was measured in the absence (solid diamonds) or presence of 24 (solid squares), 54 (solid triangles), or 108 nM (solid circles) UHDBT. After adding substrate and UHDBT to the reaction mixture, the reaction was started by the addition of the complex to a concentration of 2.5 nM. The double-reciprocal line in the absence of the inhibitor was constructed with a K_m for decyl ubiquinol of 11 μM and a V_{max} of 272 s^{-1} . The double reciprocal lines in the presence of UHDBT were constructed considering UHDBT as a competitive inhibitor with V_{max} unaltered. The resulting $K_{m(\text{app})}$ values were 37.7, 48.5, and 169 μM for 24, 54, and 108 nM UHDBT, respectively.

sionⁿ). With both donor and acceptor of the hydrogen bond being ionized, this type of hydrogen-bonded ion bridge provides a strong interaction for stabilizing ligand binding. Furthermore, this is the main interaction, which locks the catalytic Rieske domain in the b-position. Also, a weak hydrogen bond between the slightly acidic C ϵ 1 atom of His¹⁸¹ and the carbonyl O7 atom of HHDBT adds to this stabilizing effect.

Interestingly, the ionized hydroxy group of the inhibitor interacts with the phenyl ring of Tyr²⁷⁹ of cytochrome b . The ring plane of the inhibitor is at a 90° angle on-edge to the aromatic side chain of Tyr²⁷⁹ (Fig. 3). The distances between the O6 atom of HHDBT and the Tyr²⁷⁹ side chain atoms, C δ 1 and C ϵ 1, respectively, are well below the sum of their van der Waals radii ($d_{\text{C}\delta\text{1-O6}} = 3.2 \text{ \AA}$ and $d_{\text{C}\epsilon\text{1-O6}} = 3.3 \text{ \AA}$), indicating the presence of weak, nonconventional hydrogen bonds (C-H...O) with the aromatic C-H groups as donors. Hydrogen bond angles and bending angles at the acceptor atom ($\theta_{\text{C}\delta\text{1-H-O6}} = 125^\circ$, $\theta_{\text{C}\epsilon\text{1-H-O6}} = 113^\circ$, $\phi_{\text{H}\delta\text{1-O6-C6}} = 107^\circ$, $\phi_{\text{H}\epsilon\text{1-O6-C6}} = 94^\circ$) are slightly below the optimal range for nonconventional hydrogen bonds, a feature that has been observed for this type of hydrogen bond with a bifurcated acceptor (30). The bifurcation is not fully symmetrical, since conditions for the bond involving C δ 1 are more favorable. The acidity of the aromatic C-H groups is increased, because the hydroxy group of Tyr²⁷⁹ of cytochrome b donates a hydrogen bond to the backbone oxygen of Cys¹⁸⁰ of the Rieske protein ($d_{\text{OH-O}} = 2.7 \text{ \AA}$; $\phi_{\text{Cz-OH-O}} = 112^\circ$). The latter provides additional stabilization of the Rieske domain in the b-position.

Furthermore, the oxygen atom of the carbonyl group, O4, which is oriented toward heme b_L , is within hydrogen bonding distance to a water molecule, Wat⁵¹⁸, that is stabilized by a hydrogen bond with the backbone nitrogen atom of Glu²⁷² of cytochrome b . Several nonpolar interactions contribute to stabilization of the hydroxydioxobenzothiazole ring, involving the following residues of cytochrome b : Met¹³⁹, Trp¹⁴², Gly¹⁴³, Val¹⁴⁶, Ile²⁶⁹, and Pro²⁷¹. Additionally, a few van der Waals interactions with Rieske protein residues His¹⁸¹, ligand of the [2Fe-2S], and Cys¹⁸⁰ are present (Table II), demonstrating the tight interaction of the Rieske cluster-bearing domain with cytochrome b at the Q_o site. Notably, all of the residues involved in binding of the hydroxydioxobenzothiazole head group

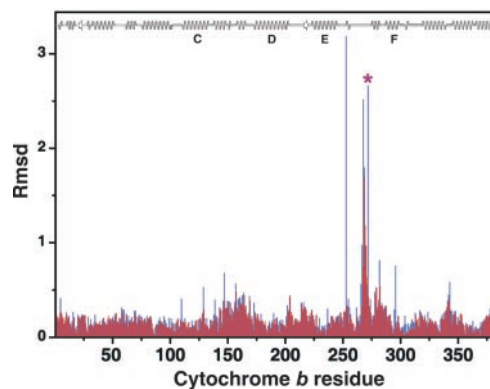


FIG. 5. Comparison of the position of cytochrome b residues from stigmatellin- and HHDBT-inhibited bc_1 complex. The root mean square deviation ($Rmsd$, \AA) of the α trace and of all atoms is depicted in red and blue, respectively. The average root mean square deviation of α atoms and of all atoms was 0.234 and 0.365 \AA , respectively. Glu²⁷² is labeled with an asterisk. The major displacements are observed in the ef loop between trans-membrane helices E and F, and subtle differences are observed for the two short helices cd1 and cd2 between C and D; notably, these residues are part of the Q_o site.

are fully conserved among mitochondrial bc_1 complexes (39). Mutations in the position of residues that are interacting with the head group, Trp¹⁴², Gly¹⁴³, Ile²⁶⁹, Pro²⁷¹, and Tyr²⁷⁹, or their homologs, result in disturbed ubiquinol occupancy and/or oxidation (40, 41). The short saturated heptyl side chain is stabilized by van der Waals interactions with cytochrome b residues Ile¹⁴⁷, Leu²⁷⁵, Phe²⁷⁸, and Met²⁹⁵.

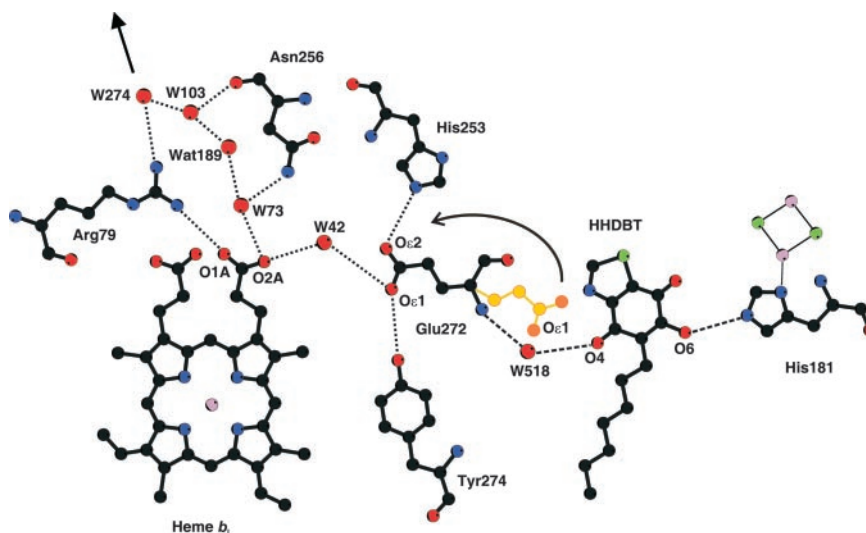
UHDBT Is a Competitive Inhibitor—To analyze whether hydroxydioxobenzothiazoles compete with substrate at the Q_o site, the apparent K_m for decyl ubiquinol binding to yeast bc_1 complex was determined at varying concentrations of UHDBT. The K_m varied with inhibitor concentration, whereas V_{max} remained constant, clearly demonstrating that UHDBT is a competitive inhibitor (Fig. 4). Therefore, hydroxydioxobenzothiazoles may be regarded as substrate analogs. High structural similarity to the substrate and competitive inhibition by HHDBT suggest that it is a substrate analogue in which the ring methyl group is replaced by a deprotonated hydroxy group, the two methoxy groups are replaced by a fused thiazole ring, and the isoprenoid tail is replaced by a short saturated side chain (see inset, Fig. 3).

Comparative Analysis of Substrate Analogs Binding at the Active Site—Stigmatellin binding to bc_1 complex was proposed to mimic the enzyme-substrate complex at an intermediate step of ubiquinol oxidation (6). The binding sites for stigmatellin and HHDBT overlap with the head groups positioned in a tight binding pocket, whereas the side chains extend into a gradually opening hydrophobic cleft. B factor analysis indicates very tight binding of stigmatellin with average B factors of 37.4 and 35.6 \AA^2 for stigmatellin and cytochrome b , respectively. HHDBT appears less tightly bound, with an average B factor_{HHDBT} of 50.9 \AA^2 and average B factor_{cytochrome b} of 40.2 \AA^2 .

Comparison of the structures of HHDBT- and stigmatellin-inhibited bc_1 complexes revealed that the major difference in α trace position and side chain orientation is confined to the direct environment of the Q_o site, notably including residues suggested by mutagenesis studies to be actively involved in Q_o site catalysis (39, 40) (Fig. 5).

The conformational changes upon HHDBT binding reveal plasticity at the Q_o site. An expansion of the binding pocket is marked by a local displacement of the α trace accompanied by altered side chain orientation of residues Ala²⁶⁷, Ser²⁶⁸, Ile²⁶⁹, and Val²⁷⁰ in a loop region close to the conserved PEWY loop

FIG. 6. Apparent hydrogen bond network at the Q_o site with the hydroxyquinone anion inhibitor bound. Glu²⁷² is hydrogen-bonded to the heme b_L propionate A, from which a proton exit pathway is formed by a chain of hydrogen-bonded water molecules, as depicted with the dotted lines. The arrow from Wat²⁷⁴ shows the proton exit pathway to bulk solvent. Hydrogen bonds stabilizing the ligand are shown as stippled lines. The position of Glu²⁷² in the stigmatellin-inhibited bc_1 complex is indicated in yellow.



(Pro²⁷¹–Tyr²⁷⁴) with maximal displacement of 1.7 Å at Ser²⁶⁸. The HHDBT head group extends deeper into the distal end of the Q_o site than the chromone ring of stigmatellin, with the Ile²⁶⁹ side chain bent away from the binding pocket. Additionally, major side chain displacements are observed for His²⁵³ and Glu²⁷². The side chains of Phe¹²⁹ and Tyr¹³² are not stabilized by interactions with HHDBT and are present in multiple conformations. Remarkably, the oxygen atom O6 of the ionized hydroxy group of HHDBT is at the same position as the carbonyl oxygen atom O8 of stigmatellin, allowing in both cases for a hydrogen bond to the Ne2 atom of His¹⁸¹ of the Rieske protein. This supports the proposal that ubiquinol binds in the same position with His¹⁸¹ as the primary ligand of the enzyme-substrate complex (6, 18, 42).

Structural Analysis of Proton Transfer Pathways—Glu²⁷² is a primary ligand of stigmatellin and was proposed to be a direct ligand of ubiquinol (6, 10). It has been suggested that Glu²⁷² releases the second proton from ubiquinol oxidation upon rotational displacement toward the heme b_L via an apparent hydrogen-bonding network established by residues Arg⁷⁹, Tyr¹³², Asn²⁵⁶, Glu²⁷², and Tyr²⁷⁴, the heme b_L propionate A, and several water molecules (6). Here, we find that the carboxylate group of Glu²⁷² is not bound to HHDBT but is dramatically rotated out of the Q_o site and that there is a hydrogen bond connecting the carboxylate to the heme propionate A (L1O2A) via a structural water molecule (Wat⁴²) (Fig. 6). The carboxylate atoms (O1ε and O2ε) of Glu²⁷² occupy the exact location of two water molecules (Wat⁴²⁸ and Wat⁵⁰) present in the stigmatellin-inhibited complex. The position of the Glu²⁷² carboxylate group in the stigmatellin structure is now occupied by a water molecule Wat⁵¹⁸, which is hydrogen-bonded to the carbonyl O4 atom of HHDBT and the backbone nitrogen atom of Glu²⁷² (Fig. 6). The reorientation of Glu²⁷² creates a rearrangement in the hydrogen bond network. Tyr²⁷⁴ remains in position and stabilizes Glu²⁷² via a hydrogen bond to the carboxylate group. His²⁵³ is rotationally displaced and forms a second hydrogen bond to the Glu²⁷² carboxylate. In this position, the Glu²⁷² protonated upon ubiquinol oxidation can deliver the proton directly to heme propionate A via the water molecule Wat⁴². Arg⁷⁹ is hydrogen-bonded to the heme propionate and provides a proton exit pathway to the bulk solvent mediated by a chain of hydrogen-bonded water molecules. The residues Arg⁷⁹, Glu²⁷², and Tyr²⁷⁴ are fully conserved in mitochondrial cytochrome *b* (39), supporting their importance for the catalytic mechanism.

Assignment of a Tightly Bound Phospholipid at the Q_o Site—Phospholipids are essential for bc_1 complex activity (35, 36).

Distinct binding sites for five phospholipid molecules have been described for the yeast complex, suggesting a specific role for the structural and functional integrity of the enzyme (7). The higher activity of the enzyme preparation used in this study was linked to less delipidation. In line with this assumption, additional tightly bound phospholipid molecules were visible in the crystal structure. Close to the Q_o site, a phospholipid molecule, tentatively assigned as a phosphatidylcholine, is bound at the intermembrane leaflet of the phospholipid bilayer. It binds in a hydrophobic cleft at the interface between cytochromes *b* and *c*₁. Binding of the head group is stabilized by interactions with the highly conserved His¹⁸⁵ of cytochrome *c*₁ and by cytochrome *b* residue Ser²⁶⁸. Phosphatidylcholine covers the protein surface at the Q_o site. The acyl chains are in contact with Trp²⁷³ of the conserved PEWY loop and attached to the displaced loop region (Ala²⁶⁷–Val²⁷⁰), pointing out that the conformational rearrangement takes place in the trans-membrane region.

This is the first phospholipid characterized that binds to the protein surface in the position of the intermembrane bilayer leaflet (Fig. 1). The acyl chains extend to be in contact with the acyl chains of the oppositely oriented matrix leaflet. The distance between the phosphodiester groups of phosphatidylcholine and the oppositely oriented phospholipids, cardiolipin and phosphatidyl ethanolamine, is 36 Å. This is in good agreement with the experimentally determined thickness of pure phosphatidylcholine bilayers with 18:1 acyl chains, where 38 Å were measured between the phosphodiester groups and 27 Å for the hydrophobic core (43). These lipids form a mediating layer to the membrane-spanning part of the protein and help to position the complex vertically in the lipid bilayer. Since HHDBT and stigmatellin resemble substrate analogs, the position of the ubiquinol binding site in the phospholipid bilayer can now be determined. The positions of the functional groups of the ligand are 6 Å below the phosphodiester group, thereby positioning the ligand at the border between the hydrophobic core and the polar zone of the head group region.

DISCUSSION

Hydroxydioxobenzothiazoles efficiently inhibit the bc_1 complex in a pH-dependent manner (38). It was argued that low efficacy at alkaline pH could be attributed to ionization of the inhibitor due to restricted access to the binding site or to protonation of a functional group within the enzyme (38, 44). Notably, the apparent pK_a of 7.5 for inhibitor efficacy is more alkaline than the pK_a of UHDBT but closely matches the pK_a suggested for the imidazole nitrogen of His¹⁸¹ of the oxidized

Rieske protein ($pK_a = 7.6$) (45). The structural and spectroscopic analysis presented here clearly show that the alkyl hydroxydioxobenzothiazole is bound in its ionized form and is stabilized by a hydrogen bond to the protonated imidazole nitrogen of His¹⁸¹, as supported by the following evidence. HHDBT is bound in the distal domain of the binding pocket with the 6-hydroxy group facing the aqueous solution when the Rieske protein is not closing the binding site. The pK_a of the hydroxy group, determined for THDBT in detergent micelles (6.1), is below the pH (8.0) used for crystallization. It is unlikely that the pK_a of HHDBT is significantly different from the measured value; the inhibitor is therefore ionized in the open conformation.

His¹⁸¹ is expected to be protonated, because it was shown to donate a hydrogen bond to the carbonyl group of stigmatellin at half a pH unit above the pH used for HHDBT crystallization. In addition, crystallization is performed close to the pK_a of His¹⁸¹. Furthermore, the enzyme preparation is partially reduced, and the pK_a of the reduced Rieske imidazole nitrogen is far above (11.5) the crystallization conditions (45). The presence of a hydrogen bond from His¹⁸¹ to HHDBT is shown by the fact that ligand binding fixes the mobile Rieske domain in the b-position. Spectroscopic analysis shows that hydroxydioxobenzothiazole is deprotonated upon binding when added in substoichiometric amounts to the complex at $pH > pK_a$ (Fig. 2). The hydrogen bond to the protonated His¹⁸¹ in combination with the bifurcated weak hydrogen bond on-edge with Tyr²⁷⁹ stabilizes the charge on oxygen atom O6.

In the nondissociated form, HHDBT can exist as *ortho*- and *para*-quinone tautomers (38). The possibility that HHDBT is bound as *ortho*-quinone with its functional groups in the same orientation as stigmatellin can be excluded, because the hydroxy group would be facing Glu²⁷², but in the HHDBT structure this residue is rotated out of the binding pocket. There is also no indication that the binding site is occupied with a mixed population of tautomers, because all interacting residues show a defined orientation as judged from the clear cut electron density and B-factor distribution.

Stigmatellin (46) and HHDBT (Fig. 4) are both competitive inhibitors. Kinetic studies show that stigmatellin is more tightly bound than UHDBT (44, 47). Furthermore, stigmatellin binding raises the midpoint potential (E_m) of the Rieske protein by 250 mV (48), whereas for UHDBT an increase of only 70 mV was determined for the bovine enzyme (37) and for the yeast enzyme.²

The position of the Rieske protein in the HHDBT-inhibited bc_1 complex is the same as in the stigmatellin-inhibited enzyme. Almost identical stabilizing interactions between the surfaces of the Rieske protein and cytochrome *b*, including positions of hydrogen-bonded water molecules at the interface, are observed. The different effects on midpoint potentials must be directly related to differences in inhibitor binding. B factor analysis indicates tighter binding of stigmatellin compared with HHDBT, and this is supported by the relative K_i values for the two inhibitors. Stigmatellin is stabilized by strong hydrogen bonds to direct ligands on both sides of the chromone ring. In contrast, direct ligands to the head group of HHDBT are confined to the ionized hydroxy group, whereas only a water molecule is hydrogen-bonded to the carbonyl group on the other side. In addition, the more rigid side chain of stigmatellin is bent along the surface and stably held by numerous contacts to cytochrome *b*. The short alkyl chain of HHDBT extends in the same direction but terminates where the stigmatellin side chain bends. Interestingly, the side chain of stig-

matellin replaces a phospholipid molecule visible in the electron density of the HHDBT structure, indicating its strong interactions with the surface of the binding pocket (results not shown).

The difference in polarization of the hydrogen bond to His¹⁸¹ will add to the effect on the midpoint potential. The hydrogen bonding pattern to the negatively charged hydroxy group creates a lower electron-withdrawing effect. Obviously, the tight binding interactions of stigmatellin involve the whole ligand, thus explaining why its binding is not pH-dependent. In contrast, stabilization of the charged HHDBT is strongly dependent on the hydrogen bond from the protonated His¹⁸¹. This is in agreement with the higher affinity of hydroxydioxobenzothiazoles to the reduced Rieske protein independent of chain length (7–15 carbon alkyl side chains), binding 15 times more strongly to the reduced Rieske protein (37). Experimental evidence and theoretical calculations suggest that reduction of the [2Fe-2S] cluster shifts the pK_a of the cluster ligands, His¹⁶¹ and His¹⁸¹, to values above 10, obviously favoring protonation of the histidines (49, 50). Consequently, pH dependence of HHDBT binding is related to the protonation state of a functional group within the protein, namely His¹⁸¹.

From structural analysis of the hydroxyquinone anion inhibitor HHDBT and stigmatellin binding at the Q_o site, the following events for electron and proton transfer are deduced (Fig. 7). Upon entry into the binding pocket, the substrate ubiquinol is stabilized with its functional groups pointing toward the primary acceptors of the low and high potential electron transfer chains, heme b_L and the [2Fe-2S] cluster, respectively. Glu²⁷² rotates into the binding pocket and forms a hydrogen bond to the hydroxy group facing the heme b_L as visible when stigmatellin is bound at the Q_o site (6). Since the extrinsic catalytic Rieske domain is mobile and His¹⁸¹ has a pK_a of 7.5 when the cluster is oxidized (45, 49), a considerable fraction of the latter is not protonated under physiological conditions. Thus, the Rieske domain can be stabilized in the b-position by forming a hydrogen bond between deprotonated His¹⁸¹ and the hydroxy group of ubiquinol. This brings the [2Fe-2S] cluster into a suitable distance for electron transfer. The initial enzyme-substrate complex is stabilized by hydrogen bonds to the primary ligands, His¹⁸¹ and Glu²⁷², which additionally serve as primary proton acceptors as previously proposed (6, 10).

Ubiquinol is oxidized in a bifurcated manner, transferring two electrons to the [2Fe-2S] cluster and heme b_L . The mechanism and the order of events are heavily debated. Some mechanisms assume a sequential reaction in which the first electron reduces the [2Fe-2S] cluster and a relatively unstable semiquinone intermediate reduces heme b_L (10). Link (16) has proposed a sequential mechanism in which a stable semiquinone is formed and is anti-ferromagnetically coupled to the Rieske center until it is oxidized by heme b_L . The concerted mechanism assumes that neither electron is transferred independently, but rather the semiquinone is so unstable that ubiquinol cannot reduce the Rieske center unless the semiquinone reduces heme b_L (17, 19). In such a mechanism, the concentration of ubisemiquinone is so low as to be almost nonexistent.

We suggest that stigmatellin and alkyl-hydroxydioxobenzothiazoles mimic either intermediates during ubiquinol oxidation or transition state intermediates. Allowing for the possibility that a stable, anti-ferromagnetically coupled ubisemiquinone might be formed under some conditions, stigmatellin binding would mimic binding of a protonated ubisemiquinone, whereas HHDBT resembles the deprotonated form (*i.e.* the ubisemiquinone anion), as illustrated in Fig. 7, *panel 5*. In both cases, the position of the reduced Rieske protein is stabilized by the

² T. Merbitz-Zahradnik and B. Trumppower, unpublished results.

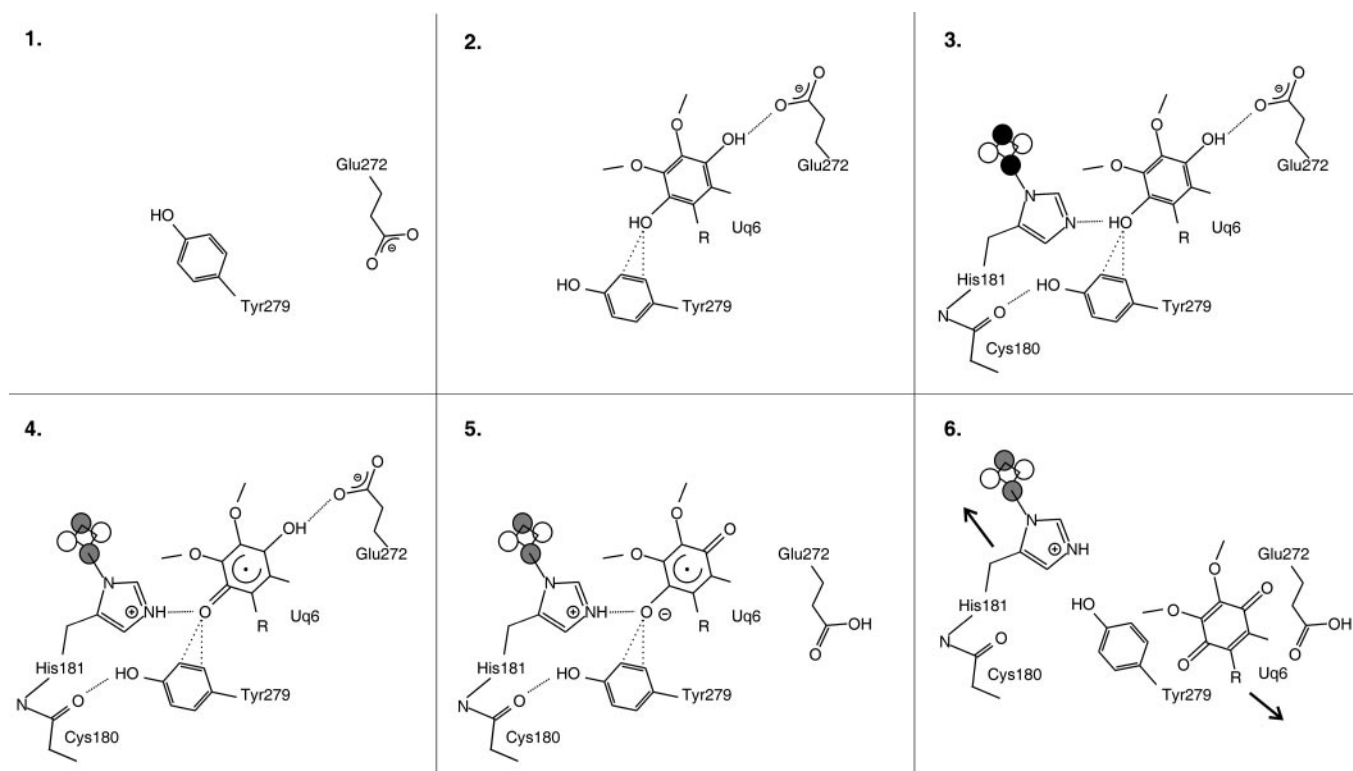


FIG. 7. **Mechanism of ubiquinol oxidation as deduced from structural analysis of hydroxyquinone anion and stigmatellin binding at the Q_o site.** The oxidized [2Fe-2S] is indicated with *black circles*; the reduced [2Fe-2S] is shown in *gray*. Hydrogen bonds stabilizing the enzyme-substrate complex as well as the b-position of the Rieske catalytic domain are indicated with *dotted lines*. *Panel 1*, empty Q_o site with Glu²⁷² directed out of the binding pocket. *Panel 2*, initial stabilization of ubiquinol by cytochrome *b* residues. *Panel 3*, the electron donor complex (“enzyme-substrate complex”) with the Rieske protein docked in the b-position. *Panel 4*, coupled electron-proton transfer to the Rieske protein as deduced from the binding mode of stigmatellin. *Panel 5*, stabilization of the anti-ferromagnetically coupled ubisemiquinone anion and rotational displacement of protonated Glu²⁷² as seen for HHDBT binding. *Panel 6*, release of the reduced and protonated Rieske protein and of the oxidized ubiquinone accompanied by displacement of Tyr²⁷⁹. Steps 4 and 5 have to be interpreted either as intermediates of a sequential reaction or as transition states intermediates as proposed by the concerted mechanism hypothesis.

hydrogen bond to His¹⁸¹. This is in agreement with EPR analysis of oriented membranes, which indicated that the reduced Rieske is preferentially located in the b-position (51).

Glu²⁷² will accept a proton from ubiquinol or ubisemiquinone and consequently rotate toward heme *b_L* as seen for HHDBT where it is not liganded to the carbonyl group. If a stable ubisemiquinone anion is formed, it is stabilized by localization of its negative charge on the oxygen atom interacting with protonated His¹⁸¹. After transfer of the second electron, the product is no longer stabilized and will leave the binding pocket and give more mobility to Tyr²⁷⁹, thus breaking its hydrogen bond to the Rieske protein (Fig. 7, panel 6). Accordingly, the latter is found to be rotated into the binding pocket in the chicken and bovine structures with an empty Q_o site (4, 5).

The importance of Tyr²⁷⁹ is supported by its full conservation in mitochondrial cytochrome *b*, and it is only replaced with a phenylalanine in a few chloroplast homologs (39). We propose that the on-edge weak hydrogen bonds from the aromatic side chain of Tyr²⁷⁹ are crucial for positioning ubiquinol in the active site. This is supported by recent mutagenesis studies in *Rhodobacter sphaeroides*, where the conservative mutation of the homologous residue Tyr³⁰³ to phenylalanine has no effect on enzyme activity, whereas exchange to Leu, Gly, and Gln resulted in a 3-, 40-, and 50-fold decrease, respectively (41).

There are two options for the final steps of substrate oxidation and product release. Either electron transfer to heme *b_L* occurs in parallel with proton transfer mediated by Glu²⁷², in which case the rotational displacement of the latter would destabilize the position of the quinone resulting in its release,

or, under conditions where a stably bound ubisemiquinone is formed, Glu²⁷² protonation and rotation occurs as a first step, and the negative charge of the ubisemiquinone anion is stabilized as seen for HHDBT. Rieske release subsequently destabilizes the charge and initiates the second electron transfer. In both cases, full oxidation of ubiquinol can take place without major repositioning of the substrate head group, as opposed to the proposed mechanism based on movement of the semiquinone in the binding pocket (10).

The two protons are released via two pathways. His¹⁸¹ releases its proton to the bulk solvent after leaving the b-position, presumably after oxidation by cytochrome *c*₁. Our studies strongly support that the rotation of Glu²⁷² is an initial step for the release of the second proton as previously proposed (6, 10, 18). Glu²⁷² is completely conserved in mitochondrial cytochrome *b* (39), and the importance of the residue for proton transfer is indicated by mutagenesis studies, since the alteration to glutamine abolishes ubiquinol oxidation in *R. sphaeroides* (40). Also, kinetic studies recently showed that protonation of a group with pK_a of 5.7 blocked catalysis, and this effect was assigned to Glu²⁷² (52). Here, the hydrogen bond rearrangements that accompany the dramatic displacement of Glu²⁷² upon HHDBT binding provide experimental evidence for the previously postulated proton transfer pathway (6). Glu²⁷² can deliver the proton directly to the heme propionate A via a single water molecule (Fig. 6). The subsequent proton release is mediated by a hydrogen-bonded water chain stabilized by cytochrome *b* residues: Arg⁷⁹, Asn²⁵⁶, Glu⁶⁶, and Arg⁷⁰.

Finally, the observed binding mode of the hydroxyquinone anion and the deduced proton transfer pathway as well as the

demonstration of competitive inhibition by HDBT suggest a feasible catalytic mechanism, which is in line with a single occupancy model for ubiquinol oxidation.

Acknowledgment—We acknowledge support by the staff of beamline ID14-EH3, ESRF (Grenoble, France).

REFERENCES

1. Brandt, U., and Trumpower, B. (1994) *Crit. Rev. Biochem. Mol. Biol.* **29**, 165–197
2. Berry, E. A., Guergova, K., Huang, L. S., and Crofts, A. R. (2000) *Annu. Rev. Biochem.* **69**, 1005–1075
3. Xia, D., Yu, C. A., Kim, H., Xia, J. Z., Kachurin, A. M., Zhang, L., Yu, L., and Deisenhofer, J. (1997) *Science* **277**, 60–66
4. Zhang, Z., Huang, L., Shulmeister, V. M., Chi, Y. I., Kim, K. K., Hung, L. W., Crofts, A. R., Berry, E. A., and Kim, S. H. (1998) *Nature* **392**, 677–684
5. Iwata, S., Lee, J. W., Okada, K., Lee, J. K., Iwata, M., Rasmussen, B., Link, T. A., Ramaswamy, S., and Jap, B. K. (1998) *Science* **281**, 64–71
6. Hunte, C., Koepke, J., Lange, C., Rossmanith, T., and Michel, H. (2000) *Struct. Fold Des.* **8**, 669–684
7. Lange, C., Nett, J. H., Trumpower, B. L., and Hunte, C. (2001) *EMBO J.* **20**, 6591–6600
8. Mitchell, P. (1976) *J. Theor. Biol.* **62**, 327–367
9. Berry, E. A., Zhang, Z., Huang, L. S., and Kim, S. H. (1999) *Biochem. Soc. Trans.* **27**, 565–572
10. Crofts, A. R., Hong, S., Ugulava, N., Barquera, B., Gennis, R., Guergova, K., and Berry, E. A. (1999) *Proc. Natl. Acad. Sci. U. S. A.* **96**, 10021–10026
11. Ding, H., Robertson, D. E., Daldal, F., and Dutton, P. L. (1992) *Biochemistry* **31**, 3144–3158
12. Ding, H., Moser, C. C., Robertson, D. E., Tokito, M. K., Daldal, F., and Dutton, P. L. (1995) *Biochemistry* **34**, 15979–15996
13. Bartoschek, S., Johansson, M., Geierstanger, B. H., Okun, J. G., Lancaster, C. R., Humpfer, E., Yu, L., Yu, C. A., Griesinger, C., and Brandt, U. (2001) *J. Biol. Chem.* **276**, 35231–35234
14. Brandt, U. (1996) *FEBS Lett.* **387**, 1–6
15. Hong, S., Ugulava, N., Guergova, K., and Crofts, A. R. (1999) *J. Biol. Chem.* **274**, 33931–33944
16. Link, T. A. (1997) *FEBS Lett.* **412**, 257–264
17. Junemann, S., Heathcote, P., and Rich, P. R. (1998) *J. Biol. Chem.* **273**, 21603–21607
18. Crofts, A. R., Barquera, B., Gennis, R. B., Kuras, R., Guergova, K., and Berry, E. A. (1999) *Biochemistry* **38**, 15807–15826
19. Snyder, C. H., Gutierrez, C., and Trumpower, B. L. (2000) *J. Biol. Chem.* **275**, 13535–13541
20. Kim, H., Xia, D., Yu, C. A., Xia, J. Z., Kachurin, A. M., Zhang, L., Yu, L., and Deisenhofer, J. (1998) *Proc. Natl. Acad. Sci. U. S. A.* **95**, 8026–8033
21. Palsdottir, H., and Hunte, C. (2003) in *Membrane Protein Purification and Crystallization: A Practical Guide*, 2nd Ed. (Hunte, C., von Jagow, G., and Schagger, H., eds) pp. 191–203, Academic Press, Inc., New York
22. Smith, P. K., Krohn, R. I., Hermanson, G. T., Mallia, A. K., Gartner, F. H., Provenzano, M. D., Fujimoto, E. K., Goeke, N. M., Olson, B. J., and Klenk, D. C. (1985) *Anal. Biochem.* **150**, 76–85
23. Otwinowski, Z., and Minor, W. (1997) *Methods Enzymol.* **276**, 307–326
24. Brunger, A. T., Adams, P. D., Clore, G. M., DeLano, W. L., Gros, P., Grosse, K., Jiang, J. S., Kuszewski, J., Nilges, M., Pannu, N. S., Read, R. J., Rice, L. M., Simonson, T., and Warren, G. L. (1998) *Acta Crystallogr. Sect. D* **54**, 905–921
25. Jones, T. A., Zou, J. Y., Cowan, S. W., and Kjeldgaard (1991) *Acta Crystallogr. Sect. A* **47**, 110–119
26. Kleywegt, G. J., and Jones, T. A. (1997) *Methods Enzymol.* **277**, 208–230
27. McDonald, I. K., and Thornton, J. M. (1994) *J. Mol. Biol.* **238**, 777–793
28. Hubbard S. J., and Thornton J. M. (1993) *Naccess*, Version 2.1.1, Department of Biochemistry and Molecular Biology, University College, London
29. Laskowski, R. A., MacArthur, M. W., Moss, D. S., and Thornton J. M. (1993) *J. Appl. Crystallogr.* **26**, 283–291
30. Desiraju, G. R., and Steiner, T. (1999) *The Weak Hydrogen Bond*, Oxford University Press, NY
31. Wallace, A. C., Laskowski, R. A., and Thornton, J. M. (1995) *Protein Eng.* **8**, 127–134
32. Kraulis, P. J. (1991) *J. Appl. Crystallogr.* **24**, 946–950
33. Esnouf, R. M. (1999) *Acta Crystallogr. Sect. D* **55**, 938–940
34. Merritt, E. A., and Murphy, M. E. P. (1994) *Acta Crystallogr. D* **50**, 869–873
35. Yu, C. A., and Yu, L. (1980) *Biochemistry* **19**, 5715–5720
36. Schagger, H., Hagen, T., Roth, B., Brandt, U., Link, T. A., and von, J. (1990) *Eur. J. Biochem.* **190**, 123–130
37. Bowyer, J. R., Edwards, C. A., Ohnishi, T., and Trumpower, B. L. (1982) *J. Biol. Chem.* **257**, 8321–8330
38. Trumpower, B. L., and Haggerty, J. G. (1980) *J. Bioenerg. Biomembr.* **12**, 151–164
39. Degli Esposti, M., De Vries, S., Crimi, M., Ghelli, A., Patarnello, T., and Meyer, A. (1993) *Biochim. Biophys. Acta* **1143**, 243–271
40. Brasseur, G., Saribaf, A. S., and Daldal, F. (1996) *Biochim. Biophys. Acta* **1275**, 61–69
41. Crofts, A. R., Guergova, K., Kuras, R., Ugulava, N., Li, J., and Hong, S. (2000) *Biochim. Biophys. Acta* **1459**, 456–466
42. Samoilova, R. I., Kolling, D., Uzawa, T., Iwasaki, T., Crofts, A. R., and Dikanov, S. A. (2002) *J. Biol. Chem.* **277**, 4605–4608
43. Lewis, B. A., and Engelman, D. M. (1983) *J. Mol. Biol.* **166**, 211–217
44. Zhang, L., Snyder, C., Trumpower, B. L., Yu, L., and Yu, C. A. (1999) *FEBS Lett.* **460**, 349–352
45. Link, T. A., Hagen, W. R., Pierik, A. J., Assmann, C., and von Jagow, G. (1992) *Eur. J. Biochem.* **208**, 685–691
46. Covian, R., Pardo, J. P., and Moreno-Sanchez, R. (2002) *J. Biol. Chem.* **277**, 48449–48455
47. Zhang, L., Tai, C. H., Yu, L., and Yu, C. A. (2000) *J. Biol. Chem.* **275**, 7656–7661
48. von Jagow, G., and Ohnishi, T. (1985) *FEBS Lett.* **185**, 311–315
49. Link, T. A. (1994) *Biochim. Biophys. Acta* **1185**, 81–84
50. Ullmann, G. M., Noodleman, L., and Case, D. A. (2002) *J. Biol. Inorg. Chem.* **7**, 632–639
51. Brugna, M., Rodgers, S., Schricker, A., Montoya, G., Kazmeier, M., Nitschke, W., and Sinning, I. (2000) *Proc. Natl. Acad. Sci. U. S. A.* **97**, 2069–2074
52. Covian, R., and Moreno, S. (2001) *Eur. J. Biochem.* **268**, 5783–5790
53. Collaborative Computational Project (1994) *Acta Crystallogr. Sect. D* **50**, 760–763